A&A 491, 767–780 (2008)
DOI: 10.1051/0004-6361:200810332

Astronomy & Astrophysics

The old Galactic open clusters FSR 1716 and Czernik 23

C. Bonatto and E. Bica

Universidade Federal do Rio Grande do Sul, Departamento de Astronomia CP 15051, RS, Porto Alegre 91501-970, Brazil
e-mail: [charles;bica;charles]@if.ufrgs.br

Received 5 June 2008 / Accepted 12 September 2008

ABSTRACT

Context. Open clusters older than ∼4 Gyr are rare in the Galaxy. Affected by a series of mass-decreasing processes, the stellar content of most open clusters dissolves into the field on a time-scale shorter than ∼1 Gyr. In this sense, improving the statistics of old objects may provide constraints for a better understanding of the dynamical dissolution of open clusters.
Aims. Our main purpose is to investigate the nature of the globular cluster candidate FSR 1716, located at $\ell = 329.8°$ and $b = -1.6°$. We also derive parameters of the anti-centre open cluster Czernik 23 (FSR 834). Both objects have been detected as stellar overdensities in the Froebrich, Scholz & Raftery star cluster candidate catalogue.
Methods. The analyses are based on near-infrared colour−magnitude diagrams and stellar radial density profiles. The intrinsic colour−magnitude diagram morphology is enhanced by a field-star decontamination algorithm applied to the 2MASS J, H, and K_s photometry.
Results. Isochrone fits indicate that FSR 1716 is more probably an old (∼7 Gyr) and absorbed ($A_V = 6.3 \pm 0.2$) open cluster, located ≈0.6 kpc inside the solar circle in a contaminated central field. However, we cannot rule out the possibility of a low-mass, loose globular cluster. Czernik 23 is shown to be an almost absorption-free open cluster, ∼5 Gyr old, located about 2.5 kpc towards the anti-centre. In both cases, solar and sub-solar ([Fe/H] ∼ −0.5) metallicity isochrones represent equally well the stellar sequences. Both star clusters have a low mass content (≲200 $M_\odot$) presently stored in stars. Their relatively small core and cluster radii are comparable to those of other open clusters of similar age. These structural parameters are probably a consequence of the several Gyr of mass loss due to stellar evolution, tidal interactions with the disk (and bulge in the case of FSR 1716), and possibly giant molecular clouds.
Conclusions. Czernik 23, and especially FSR 1716, are rare examples of extreme dynamical survivors. The identification of both as such represents an increase of ≈10% in the known population of open clusters older than ∼4 Gyr in the Galaxy.

Key words. Galaxy: open clusters and associations: general – Galaxy: open clusters and associations: individual: FSR 1716 – Galaxy: open clusters and associations: individual: Czernik 23

1. Introduction

The Galaxy is an aggressive environment for star clusters in general, open clusters (OCs) in particular. These stellar systems continually undergo a series of dynamical processes such as mass loss associated with stellar evolution, mass segregation and evaporation, tidal interactions with the Galactic disk and bulge, and collisions with giant molecular clouds. Combined over time, such processes tend to accelerate the dynamical evolution, which produces significant changes in the cluster structure and eroded mass functions. Eventually, most OCs end up completely dissolved in the Galactic stellar field or as poorly-populated remnants (Pavani & Bica 2007, and references therein).

Theoretical (e.g. Spitzer 1958; Lamers & Gieles 2006), N-body (e.g. Baumgardt & Makino 2003; Goodwin & Bastian 2006; Khalisi et al. 2007), and observational (e.g. van den Bergh 1957; Oort 1958; von Hoerner 1958; Piskunov et al. 2007) evidence indicate that the disruption-time scale near the solar circle is shorter than ∼1 Gyr. Around this region, the disruption time-scale depends on mass as $t_{dis} \sim M^{0.62}$ (Lamers & Gieles 2006), which for clusters with mass in the range 10^2–10^3 $M_\odot$ corresponds to $75 \lesssim t_{dis}(\mathrm{Myr}) \lesssim 300$. In general, the effect of the relevant dynamical processes is stronger for the OCs more centrally located and the low-mass ones (see Bonatto & Bica 2007a, for a detailed discussion on disruption effects and time-scales). Indeed, OCs older than ∼1 Gyr are preferentially found near the solar circle and in the outer Galaxy (e.g. Friel 1995; Bonatto et al. 2006a), where the frequency of potentially damaging dynamical interactions with giant molecular clouds and the disk is lower (e.g. Salaris et al. 2004; Upgren et al. 1972). Disruption efficiency increases critically towards the Galactic centre, to the point that the inner ($R_{GC} \lesssim 150$ pc) tidal fields can dissolve a massive star cluster in ∼50 Myr (Portegies Zwart et al. 2002).

The above aspects considered, the natural expectation is that only a small fraction of the OCs can reach old ages, and that the successful ones will be preferentially found at large Galactocentric distances. In fact, of the ≈1000 OCs with known age listed in the WEBDA[1] database, 180 are older than 1 Gyr, and only 18 (≈2%) are older than 4 Gyr (see also Ortolani et al. 2005a,b). Not surprisingly, most of the OCs older than 1 Gyr identified so far are located outside the solar circle (see, e.g., the spatial distribution of OCs of different ages in Fig. 1 of Bonatto & Bica 2007a).

In this context, it is naturally expected that the discovery and derivation of astrophysical parameters of old OCs will better define the OC parameter space. Thus, a better understanding of the dynamical survival rate of star clusters in the tidal field of the Galaxy can be reached. Such parameters, in turn, can be used in

[1] obswww.univie.ac.at/webda – Mermilliod & Paunzen (2003).

studies of star formation and evolution processes, dynamics of N-body systems, and the geometry of the Galaxy, among others.

In the present paper we study two stellar overdensities listed in the star cluster candidate catalogue of Froebrich et al. (2007a), which turn out to be very old star clusters. They are FSR 1716 and FSR 834. The present work employs near-IR J, H, and K_s photometry obtained from the 2MASS[2] Point Source Catalogue (PSC). The spatial and photometric uniformity of 2MASS, which allow extraction of wide surrounding fields that provide high star-count statistics, are important to derive cluster parameters and probe the nature of stellar overdensities (e.g. Bica et al. 2008). For this purpose we have developed quantitative tools to statistically disentangle cluster evolutionary sequences from field stars in colour−magnitude diagrams (CMDs). We apply *(i)* field-star decontamination to quantify the statistical significance of the CMD morphology, which is important to derive reddening, age, and distance from the Sun; and *(ii)* colour−magnitude filters, which are essential for intrinsic stellar radial density profiles (RDPs), as well as luminosity and mass functions (MFs). In particular, field-star decontamination constrains the age and distance more, especially for low-latitude OCs (Bonatto et al. 2006a).

This paper is organised as follows. Section 2 contains basic properties and reviews literature data (when available) on both star cluster candidates. In Sect. 3 we present the 2MASS photometry and build the stellar surface-density distribution in the direction of both objects. In Sect. 4 we build CMDs, discuss the field-star decontamination algorithm, and provide tests of the old age of both clusters. In Sect. 5 we derive cluster fundamental parameters. Section 6 describes cluster structure by means of stellar RDPs. In Sect. 7 mass functions are built and cluster masses are estimated. In Sect. 8 aspects related to the structure and dynamical state of the present clusters are considered. Concluding remarks are given in Sect. 9.

2. FSR 1716 and FSR 834 as stellar overdensities

The catalogue built by Froebrich et al. (2007a) includes 1021 star cluster candidates (hereafter FSR objects) for Galactic latitudes $|b| < 20°$ and all longitudes. The targets were selected by an automated algorithm that identifies small-scale regions that present stellar overdensities, applied to the 2MASS database. The overdensities are classified according to a quality flag, "0" and "1" for the most probable star clusters, and "5" and "6", which may be related to field fluctuations. Based on a combination of the number of cluster stars (corrected to a common magnitude limit), the core radius and the central star density, Froebrich et al. (2007a) could discriminate known globular clusters (GCs) from OCs. With this criterion applied to the overdensity catalogue, they found 1012 OC and 9 GC candidates.

Several studies have explored the FSR catalogue with different approaches, with results that reflect the importance of such a catalogue. The recently discovered GCs FSR 1735 (Froebrich et al. 2007b) and FSR 1767 (Bonatto et al. 2007), and the probable GCs FSR 584 (Bica et al. 2007) and FSR 190 (Froebrich et al. 2008), are clear examples of the fundamental rôle played by the FSR catalogue in improving the statistics of very old star clusters. Indeed, FSR 1735 and FSR 1767 are the most recent additions to the Galactic GC population, currently of ∼160 members (e.g. Bonatto & Bica 2008a). On the other hand, the decontamination algorithm (Sect. 4) applied to the 2MASS photometry of some FSR GC candidates has shown that FSR 89 (Bonatto & Bica 2007a) and FSR 1603 (Bica & Bonatto 2008) are open clusters of age ∼1 Gyr, while FSR 1755 appears to be an embedded OC (Bica & Bonatto 2008).

During a close investigation of the overdensities, we noted that the CMDs of FSR 1716 and FSR 834 show features typical of old stellar systems. Indeed, FSR 1716 was classified as a GC candidate by Froebrich et al. (2007a). FSR 1716, at $\ell = 329.79°$ and $b = -1.59°$ is projected not far from the Galactic centre, which implies the presence of significant contamination by bulge stars. FSR 834, on the other hand, is a disk object projected towards the anti-centre ($\ell = 180.55°$ and $b = +0.82°$). It has the poorly-studied OC Czernik 23 (hereafter Cz 23) as an optical counterpart. Czernik (1966) measured a diameter of 5′ and estimated that Cz 23 contains about 40 member stars, and Ruprecht (1966) classified it as III 1p.

Figure 1 (left panel) shows a $4' \times 4'$ 2MASS K_s image of FSR 1716, where a significant concentration of stars is superimposed on a relatively crowded field, as expected from such a central direction. For Cz 23 we show in the right panel a $7' \times 7'$ XDSS[3] R band image. In this case the cluster can be easily seen against a relatively clean field.

Table 1 provides fundamental data on both objects. Coordinates from Froebrich et al. (2007a) are given in Cols. 2 to 5; their quality flag in is Col. 6, and the core and tidal radii measured in the H band are given in Cols. 7 and 8. The age, central reddening, distance from the Sun, Galactocentric distance, and the components projected onto the Galactic plane derived in the present study (Sect. 5) are given in Cols. 9 to 16.

3. 2MASS photometry

2MASS photometry in the J, H, and K_s bands was extracted in circular fields of extraction radius R_{ext} centred on the coordinates of the objects (Table 1) by means of VizieR[4]. Previous studies with OCs in different environments (Sect. 1) revealed that in the absence of a neighbouring populous cluster and important differential absorption, wide extraction areas provide suitable statistics for a consistent characterisation of the field stars in terms of colour and magnitude. Based on this premise we adopted an extraction radius of $R_{ext} = 30'$, which is beyond the cluster radius (Sect. 6 and Col. 9 of Table 3) of the present objects. For decontamination purposes, comparison fields were extracted within wide rings located beyond the cluster radii. As a photometric quality constraint, the 2MASS extractions were restricted to stars *(i)* brighter than those of the 99.9% Point Source Catalogue completeness limit[5] in the cluster direction; and *(ii)* with errors in J, H, and K_s smaller than 0.3 mag. The 99.9% completeness limits refer to field stars, and depend on Galactic coordinates. In the present cases, the fraction of stars with J, H, and K_s uncertainties smaller than 0.06 mag is ≈80%. A typical distribution of uncertainties as a function of magnitude, for objects projected towards the central parts of the Galaxy, can be found in Bonatto & Bica (2007b). Reddening transformations use the relations $A_J/A_V = 0.276$, $A_H/A_V = 0.176$, $A_{K_s}/A_V = 0.118$, and $A_J = 2.76 \times E(J-H)$ (Dutra et al. 2002), for a constant

[2] The Two Micron All Sky Survey, All Sky data release (Skrutskie et al. 1997), available at http://www.ipac.caltech.edu/2mass/releases/allsky/

[3] Extracted from the Canadian Astronomy Data Centre (CADC), at http://cadcwww.dao.nrc.ca/

[4] http://vizier.u-strasbg.fr/viz-bin/VizieR?-source=II/246

[5] http://www.ipac.caltech.edu/2mass/releases/allsky/doc/

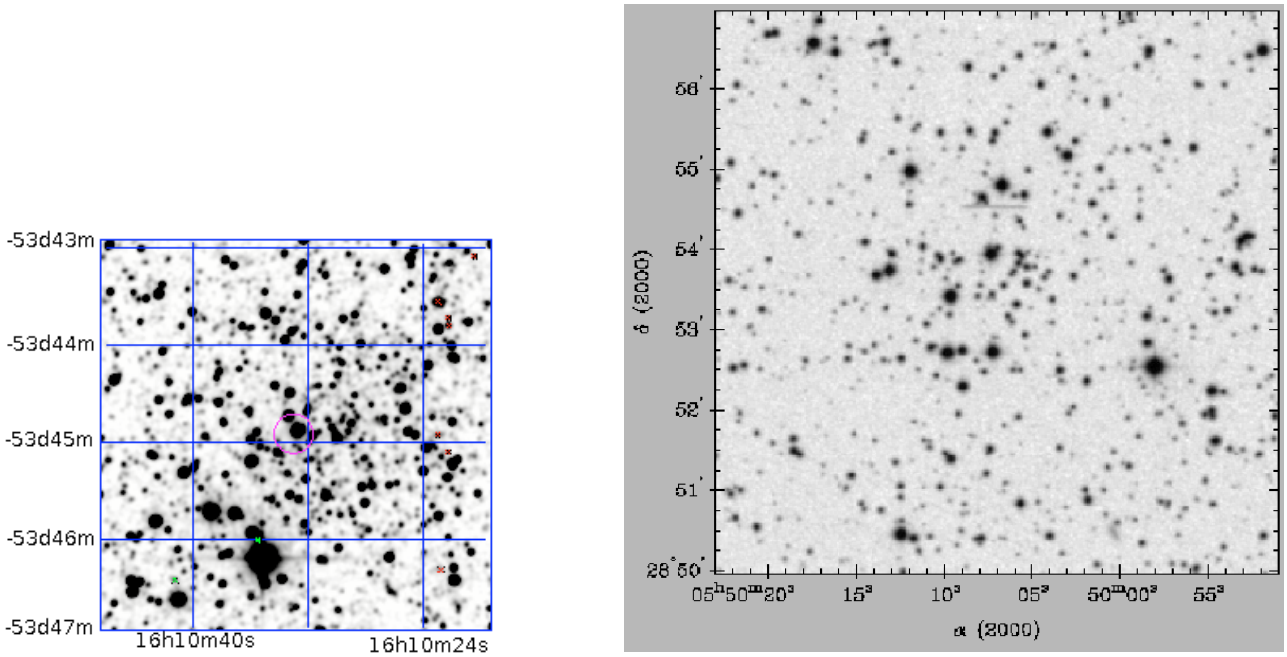

Fig. 1. *Left panel*: 4′ × 4′ 2MASS K_s image of FSR 1716. Image provided by the 2MASS Image Service. The small circle indicates the central coordinates (Cols. 2 and 3 of Table 1). *Right panel*: 7′ × 7′ XDSS *R* image of Cz 23. North is to *the top and East to the left*.

Table 1. General data on the clusters.

	FSR2007							This paper						
cluster	α(2000)	δ(2000)	ℓ	b	Q	$R_{c,H}$	$R_{t,H}$	Age	A_V	$d_\odot$	R_{GC}	X_{GC}	Y_{GC}	Z_{GC}
	(hms)	(° ′ ″)	(°)	(°)		(′)	(′)	(Gyr)	(mag)	(kpc)	(kpc)	(kpc)	(kpc)	(kpc)
(1)	(2)	(3)	(4)	(5)	(6)	(7)	(8)	(9)	(10)	(11)	(12)	(13)	(14)	(15)
FSR 1716†	16:10:33	−53:44:12	329.79	−1.59	2	1.2	5.9	7.0 ± 1.0	6.3 ± 0.2	0.8 ± 0.1	6.6 ± 0.1	−6.6 ± 0.1	−0.37 ± 0.04	−0.02 ± 0.01
FSR 1716‡	16:10:33	−53:44:12	329.79	−1.59	2	1.2	5.9	12.0 ± 2.0	6.3 ± 0.4	2.3 ± 0.3	5.4 ± 0.3	−5.3 ± 0.3	−1.13 ± 0.17	−0.06 ± 0.01
Cz 23	05:50:07	+28:53:28	180.55	+0.82	1	0.8	4.2	5.0 ± 1.0	0.0 ± 0.1	2.5 ± 0.1	9.7 ± 0.2	−9.7 ± 0.1	−0.02 ± 0.01	+0.04 ± 0.01

Notes. Coordinates (Cols. 2 to 5), quality flag (Col. 6), and core and tidal radii (Cols. 7 and 8) measured in the *H* band are from Froebrich et al. (2007a); Col. 10: reddening towards the cluster's central region (Sect. 5); Col 11: distance from the Sun; Col. 12: cluster Galactocentric distance for $R_\odot$ = 7.2 kpc (Bica et al. 2006a); Cols. 13–15: coordinate components projected onto the Galactic plane. Cz 23 is the optical counterpart of FSR 834. Parameters of FSR 1716 are derived for the OC (†) or globular cluster (‡) interpretation (Sect. 5).

total-to-selective absorption ratio R_V = 3.1. These ratios were derived from the extinction curve of Cardelli et al. (1989).

As a first step in understanding the nature of both overdensities, we show in Fig. 2 the spatial distribution of the stellar surface-density as measured with 2MASS photometry. In both cases we compute the surface density (σ, in units of stars arcmin^{-2}) in a rectangular mesh with cells of dimensions 4′ × 4′. The mesh reaches total offsets of $|\Delta\alpha| = |\Delta\delta| \approx 20'$ with respect to the centre, in right ascension and declination. Since the cluster radius of both objects is $\lesssim$6′ (Table 3), most of the cluster structure should be contained in the central cell. Because of the significant contamination by field stars, the surface-density built with the observed (raw) photometry of the centrally projected OC FSR 1716 is very irregular (top-left panel), although an excess can be seen in the central cell, which corresponds to the overdensity detected by Froebrich et al. (2007a). Cz 23, on the other hand, clearly stands out in the central cell (top-right panel) against a less-irregular field. The bottom panels show the surface densities built with field-star decontaminated photometry (Sect. 4).

4. Field-star decontamination

Especially in the case of FSR 1716, the stellar surface-density in the direction of both objects clearly shows that field-star contamination should be taken into account. This assertion is further supported by the $J \times (J-H)$ and $J \times (J-K_s)$ CMDs extracted from the $R < 3'$ region of FSR 1716 (Fig. 3), and the $R < 4'$ region of Cz 23 (Fig. 4). Features present in the central CMDs and in the respective comparison field (top and middle panels) show that field stars contribute in varying proportions to the CMDs, especially for the bulge-projected FSR 1716. Nevertheless, when contrasted with the equal-area comparison field extractions, sequences typical of old stellar systems are suggested in both cases – a conspicuous giant branch in FSR 1716 and a giant clump in Cz 23.

Field-star decontamination is a very important, yet difficult, step in the identification and characterisation of star clusters. Different approaches have been used for this, among them, those of Mercer et al. (2005) and Carraro et al. (2006). The first is based on spatial variations of the star-count density, but does not take into account CMD properties. In the latter, stars in a

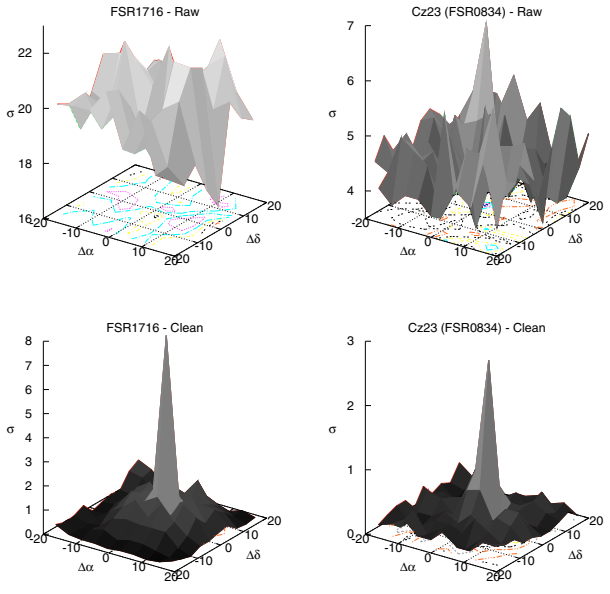

Fig. 2. Stellar surface-density σ(stars arcmin^{-2}) of FSR 1716 (*left panels*) and Cz 23 (*right*). The curves were computed for a mesh size of $4' \times 4'$, centred on the coordinates in Table 1. The observed (raw) and field-star decontaminated photometry are shown in *the top and bottom panels*, respectively.

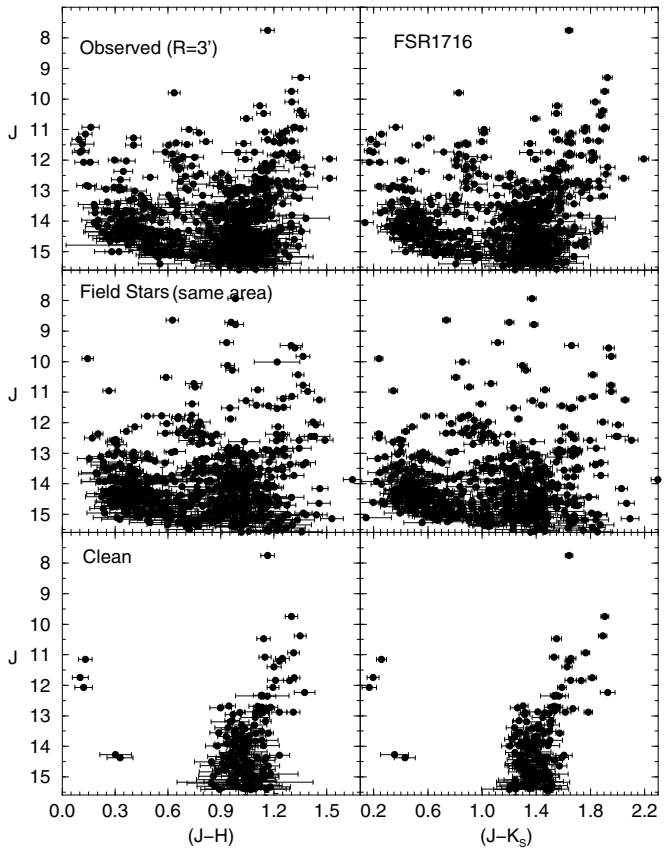

Fig. 3. 2MASS CMDs extracted from the $R < 3'$ region of FSR 1716. *Top panels*: observed photometry with the colours $J \times (J-H)$ (*left*) and $J \times (J-K_s)$ (*right*). *Middle*: equal-area ($19.77' < R < 20'$) extraction of the comparison field, where the significant disk and bulge contamination can be seen. *Bottom panels*: decontaminated CMDs that reveal a highly reddened, relatively populous MS and a giant branch, typical of old clusters.

CMD extracted from an assumed cluster region are subtracted according to colour and magnitude similarity with the stars of an equal-area comparison field CMD.

In the present case, we apply the statistical algorithm described in Bonatto & Bica (2007b) to quantify the field-star contamination in the CMDs. The algorithm makes use of both approaches above, in the sense that the relative star-count density together with colour/magnitude similarity between cluster and comparison field extractions are taken into account simultaneously. It measures the relative number densities of probable field and cluster stars in cubic CMD cells whose axes correspond to the J magnitude and the $(J-H)$ and $(J-K_s)$ colours. These are the 2MASS colours that provide the maximum variance among CMD sequences for OCs of different ages (e.g. Bonatto et al. 2004). The algorithm: *(i)* divides the full range of magnitude and colours covered by the CMD into a 3D grid, *(ii)* calculates the expected number density of field stars in each cell based on the number of comparison field stars with similar magnitude and colours as those in the cell; and *(iii)* subtracts the expected number of field stars from each cell. The algorithm is responsive to local variations of field-star contamination (Bonatto & Bica 2007b). Typical cell dimensions are $\Delta J = 1.0$, and $\Delta(J-H) = \Delta(J-K_s) = 0.25$, which are wide enough to allow for sufficient star-count statistics in individual cells and narrow enough to preserve the morphology of the CMD evolutionary sequences. The comparison fields are located within $R = 15'$–$30'$ (FSR 1716), and $R = 10'$–$30'$ (Cz 23). In both cases, the inner boundary of the comparison field lies beyond the probable tidal radius (Sect. 6), which minimises the probability of oversubtraction of member stars. We emphasise that the equal-area field extractions shown in the middle panels of Figs. 3 and 4 serve only for comparisons among the panels. Actually, the decontamination process is carried out with the wide surrounding area as described above. Further details on the algorithm, including discussions on subtraction efficiency and limitations, are given in Bonatto & Bica (2007b).

As extensively discussed in Bonatto & Bica (2007b), differential reddening between cluster and field stars is critical for the decontamination algorithm. Large gradients would require wide cell sizes or, in extreme cases, would preclude application of the algorithm altogether. It would require, e.g. a $|\Delta(J-H)| \gtrsim$ cell size (0.25, in the present work) between cluster and comparison field for the differential reddening to affect the subtraction in a given cell. However, in both cases the CMDs extracted from the cluster region and comparison field (Figs. 3 and 4) indicate that the differential reddening, if present, is not important.

The decontaminated stellar surface-density distributions (bottom panels of Fig. 2) are an indicator of the algorithm efficiency. In both cases the central cells, which correspond to the location of the overdensities, present conspicuous surface densities. Also, the residual surface-density around the centre was reduced to a minimum level. We note that the decontamination is essentially based on the colour–magnitude distributions of the stars in different spatial regions. The fact that the decontaminated surface density has a conspicuous excess only at the assumed cluster region (Fig. 2) implies significant differences among the spatial regions, both in the colour–magnitude distributions and in the number of stars within a given colour–magnitude bin. This is expected of star clusters, which can be characterised by a single stellar population, projected against a Galactic stellar field.

Table 2. Statistics of the field-star decontamination discriminated by magnitude bins.

ΔJ	FSR 1716 ($R < 3'$)					Cz 23 ($R < 4'$)				
(mag)	N_{obs} (stars)	N_{cl} (stars)	$N_{1\sigma}$	σ_{FS} (stars)	FS_{unif}	N_{obs} (stars)	N_{cl} (stars)	$N_{1\sigma}$	σ_{FS} (stars)	FS_{unif}
7–8	1 ± 1.0	1	1.0	0.20	0.36	—	—	—	—	—
8–9	1 ± 1.0	1	1.0	0.38	0.23	—	—	—	—	—
9–10	3 ± 1.7	1	0.6	0.37	0.08	2 ± 1.4	1	0.7	0.47	0.63
10–11	11 ± 3.3	3	0.9	0.81	0.07	7 ± 2.6	6	2.3	0.91	0.38
11–12	37 ± 6.1	9	1.5	1.90	0.07	1 ± 1.0	0	0.0	1.08	0.22
12–13	82 ± 9.1	20	2.2	3.23	0.05	10 ± 3.2	2	0.6	1.50	0.15
13–14	145 ± 12.0	36	3.0	6.33	0.05	24 ± 4.9	5	1.0	2.33	0.11
14–15	248 ± 15.7	57	3.6	8.45	0.04	66 ± 8.1	22	2.7	3.77	0.08
15–16	—	—	—	—	—	118 ± 10.9	30	2.8	5.61	0.07
All	528 ± 23.0	128	5.0	19.2	0.04	228 ± 15.1	66	4.4	15.6	0.07

Notes. The table provides, for each magnitude bin (ΔJ), the number of observed stars (N_{obs}) within the spatial region sampled in the CMDs shown in the top panels of Figs. 3 and 4, the respective number of probable member stars (N_{cl}) computed by the decontamination algorithm, the $N_{1\sigma}$ parameter, the 1σ Poisson fluctuation (σ_{FS}) around the mean, with respect to the star counts measured in the 8 sectors of the comparison field, and the field-star uniformity parameter. The statistical significance of N_{cl} is reflected in its ratio with the 1σ Poisson fluctuation of N_{obs} ($N_{1\sigma}$) and with σ_{FS}. The bottom line corresponds to the full magnitude range.

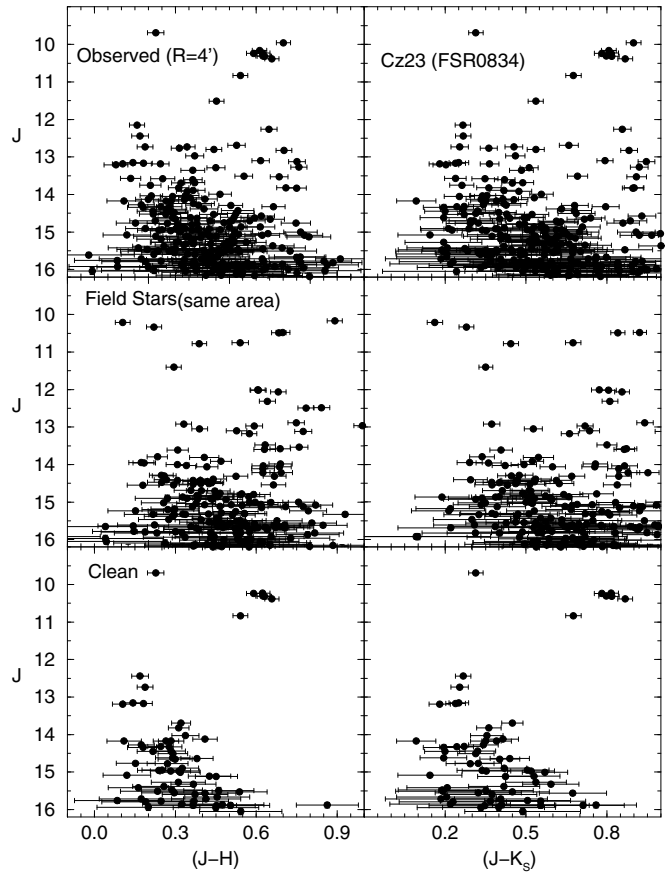

Fig. 4. Same as Fig. 3 for the region $R < 4'$ of Cz 23. Contamination, in this case, is less. The equal-area comparison field extraction was taken from the region $19.6' < R < 20'$. A giant clump shows up especially in the decontaminated CMDs, denoting advanced age.

The decontaminated CMDs are shown in the bottom panels of Figs. 3 and 4. As expected, essentially all of the bulge and disk contamination in FSR 1716 is removed, leaving stellar sequences typical of a reddened old OC, with a rather populous main sequence (MS), well-defined main sequence turnoff (MSTO), and the giant branch. Alternatively, the decontaminated morphology might resemble that of a poorly-populated GC. We explore this possibility in Sect. 5.1. Of the 588 stars present in the $R < 3'$ CMD, only 128 remain. A similar conclusion applies to Cz 23, in which the disk contamination has been subtracted, revealing a poorly-populated, old OC; 66 of the 228 stars remain in the CMD after decontamination.

The approximately central direction of FSR 1716 and the poorly-populated nature of Cz 23 require additional statistical analysis. For this purpose, we present in Table 2 the full statistics of the decontaminated sequences and field stars, discriminated by magnitude bins. Statistically relevant parameters that characterise the nature of a star cluster are: *(i)* $N_{1\sigma}$ which, for a given magnitude bin, corresponds to the ratio of the decontaminated number of stars to the 1σ Poisson fluctuation of the number of observed stars; *(ii)* σ_{FS}, which is related to the probability that the decontaminated stars result from the normal star count fluctuation in the comparison field and; *(iii)* FS_{unif}, which measures the star-count uniformity of the comparison field. Properties of $N_{1\sigma}$, σ_{FS}, and FS_{unif}, measured in OCs and field fluctuations are discussed in Bica et al. (2008). Table 2 also provides integrated values of the above parameters, which correspond to the full magnitude range spanned by the CMD of each OC. The spatial regions considered here are those sampled by the CMDs shown in the top panels of Figs. 3 and 4.

Star cluster CMDs should have integrated $N_{1\sigma}$ values significantly higher than 1 (Bica et al. 2008), a condition that is met by FSR 1716 ($N_{1\sigma} = 5.0$) and Cz 23 ($N_{1\sigma} = 4.4$). Also, the number of decontaminated stars in each magnitude bin of FSR 1716 is higher (at the 3σ level or higher) than what could be expected from field-star fluctuations. As a further test of the statistical significance of the above results we investigate star count properties of the field stars. First, the comparison field is divided into 8 sectors around the cluster centre. Next, we compute the parameter σ_{FS}, which is the 1σ Poisson fluctuation around the mean of the star counts measured in the 8 sectors of the comparison field (corrected for the different areas of the sectors and cluster extraction). In a spatially uniform comparison field, σ_{FS} is expected to be low. In this context, star clusters should have probable number of member stars (N_{cl}) higher than $\sim 3\,\sigma_{FS}$, to minimise the probability that N_{cl} arises from fluctuations of a non-uniform comparison field. This condition is fully satisfied, in some cases reaching the level $N_{cl} \sim 5\,\sigma_{FS}$. The ratio decreases somewhat for Cz 23, probably because it has a low number of member stars. We also provide in Table 2 the parameter FS_{unif}. For a given magnitude

bin we first compute the average number of stars over all sectors $\langle N\rangle$ and the corresponding 1σ fluctuation $\sigma_{\langle N\rangle}$; thus, FS_{unif} is defined as $FS_{unif} = \sigma_{\langle N\rangle}/\langle N\rangle$. Non-uniformities such as heavy differential reddening should result in high values of FS_{unif}.

Since we usually work with comparison fields wider than the possible-cluster extractions, the correction for the different spatial areas between field and cluster is expected to produce a fractional number of probable field stars ($n^{cell}_{fs\_exp}$) in some cells. Before the cell-by-cell subtraction, the fractional numbers are rounded off to the nearest integer, but limited to the number of observed stars in each cell $n^{cell}_{fs\_sub} = NI(n^{cell}_{fs\_exp}) \leq n^{cell}_{obs}$, where NI represents the nearest integer. The global effect is quantified by means of the difference between the expected number of field stars in each cell ($n^{cell}_{fs\_exp}$) and the actual number of subtracted stars ($n^{cell}_{fs\_sub}$). Summed over all cells, this quantity provides an estimate of the total subtraction efficiency of the process,

$$f_{sub} = 100 \times \sum_{cell} n^{cell}_{fs\_sub} / \sum_{cell} n^{cell}_{fs\_exp} \quad (\%).$$

Ideally, the best results would be obtained for an efficiency $f_{sub} \approx 100\%$. With the assumed grid settings for the decontamination of FSR 1716 and Cz 23, the subtraction efficiencies turned out to be higher than 93%.

The qualitative and quantitative expectations of the decontamination algorithm have been met by the output. On the one hand, the decontaminated photometry reveals a very high excess in the surface-density distributions with respect to the surroundings, in both cases (Fig. 2). In addition, CMDs extracted from the spatial regions where the excesses occur present statistically significant (Table 2) cluster-like features (Figs. 3 and 4).

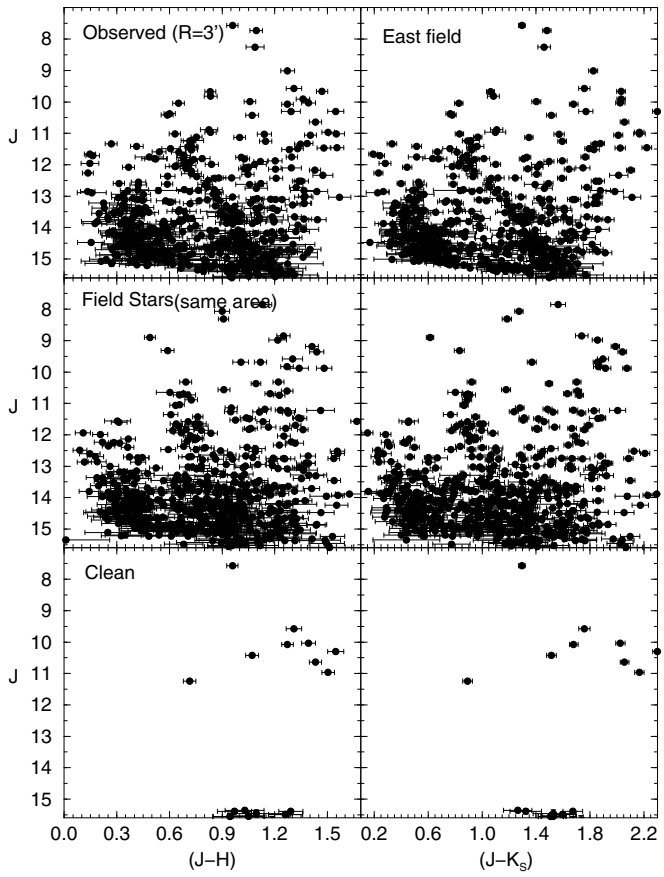

Fig. 5. Same as Fig. 3 for the $R < 3'$ region of a "test-field" located at 1° to the East of FSR 1716. The decontaminated CMDs (*bottom panels*) contain essentially statistical noise.

4.1. Additional test for FSR 1716: field at 1° to the East

Evidence drawn from the previous sections indicates that FSR 1716 is an old star cluster. However, since it lies at a low latitude and is projected not far from the dense bulge stellar field, we provide an additional test to further probe its nature. A "test-field" of 20′ of radius was extracted at 1° to the East of FSR 1716, with Galactic coordinates $\ell = 330.79°$ and $b = -1.59°$, thus projected somewhat closer to the centre than FSR 1716. The "test-field" photometry was analysed in the same way as that of FSR 1716. Similarly to FSR 1716, we considered a central region ($R < 3'$) of the "test-field", extracted the equal-area comparison field near the border (19.77′–20′), and applied the decontamination algorithm. The results are shown in Fig. 5. Contrarily to the old-cluster decontaminated CMD morphology of FSR 1716 (Fig. 3), the decontaminated CMD of the "test-field" (bottom panels of Fig. 5) contains Poisson noise produced by the mutual subtraction of star samples that share similar distributions of magnitude and colours. The same conclusion can be drawn from the featureless "test-field" RDP (Sect. 6; Fig. 10).

As discussed in Bica et al. (2008), Poisson fluctuations of the dense stellar field projected towards the bulge do not produce cluster-like CMDs and RDPs simultaneously. In particular, when field-fluctuation CMDs are field-star decontaminated, what results is represented by the above FSR 1716 "test-field" experiment (Fig. 5). In this sense, the striking differences exhibited by the CMD and RDP of FSR 1716, as compared to those of the "test-field", can be taken as robust evidence of the old-cluster nature of FSR 1716.

4.2. Additional comparison fields for Cz 23

The CMD of Cz 23, especially the decontaminated one (Fig. 4), suggests a poorly-populated old OC. Thus, we test whether the decontamination procedure, applied to random fields around Cz 23, produces similar cluster-like sequences and stellar radial profiles. We consider $R = 4'$ comparison fields, taken at 20′ to each side of Cz 23. These fields have the same projected area as that of Cz 23 shown in Fig. 4, and the centre to centre offsets correspond to ≈4 times the cluster radius of Cz 23 (Table 3). Field-star decontamination was applied to these CMDs using the same offset field as that employed for Cz 23 (Sect. 4), but restricted to $R = 25'–30'$ to avoid self subtraction.

The observed and decontaminated comparison field CMDs are shown in Fig. 6. In stark contrast to the decontaminated CMD of Cz 23 (Fig. 4), what remains in the $R = 4'$ comparison field CMDs is a randomly scattered small number of stars, similar to the CMD of the FSR 1716 "test-field" (Sect. 4.1). To complete this analysis we also include in Fig. 6 the RDPs of the comparison fields. Both CMDs and RDPs of the comparison fields are typical of Poisson fluctuations of stellar fields projected towards the Galactic anti-centre (Bonatto & Bica 2008b).

As expected of field fluctuations, the CMDs and RDPs of the comparison fields (Fig. 6) are featureless, in contrast to the cluster CMD (Fig. 4) and RDP (Fig. 11) of Cz 23.

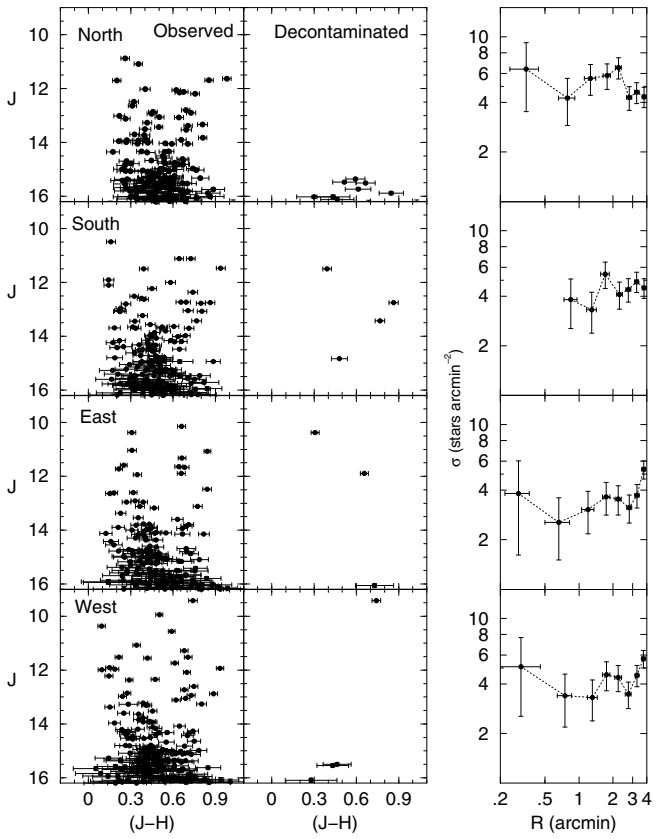

Fig. 6. *Left panels*: observed and decontaminated CMDs extracted from $R = 4'$ comparison fields, taken at $20'$ to each side of Cz 23. The corresponding RDPs (*right panels*) exhibit mainly field-fluctuation features.

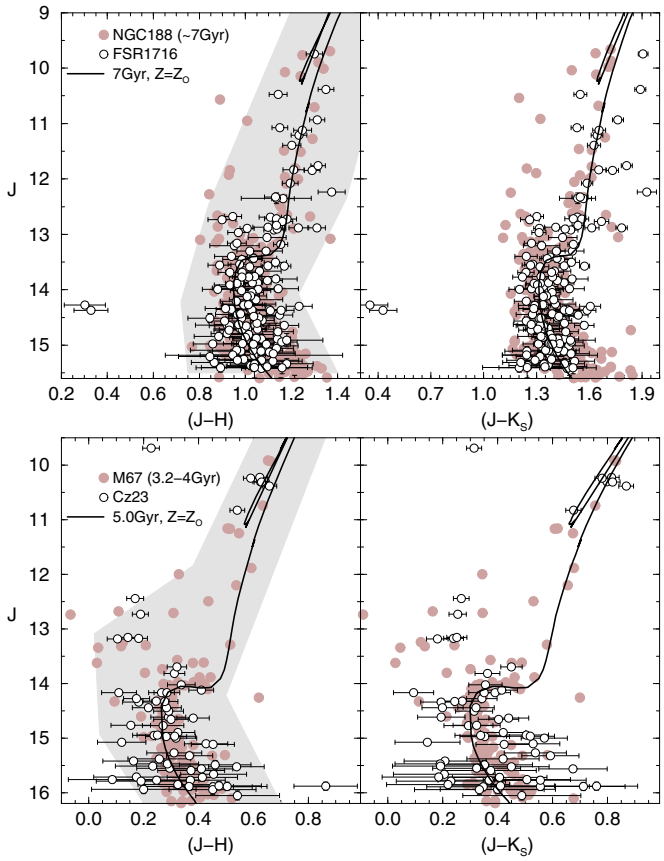

Fig. 7. *Top panels*: the field-decontaminated ($R < 3'$) CMD morphology of FSR 1716 (empty circles) is compared to that of the ~7 Gyr OC NGC 188 (gray circles). $J \times (J-H)$ (*left panels*) and $J \times (J-K_s)$ (*right*) CMDs are shown. *Bottom*: same as above for the $R < 4'$ CMD of Cz 23 (empty circles) and M 67 (gray circles). The *adopted fit* (Sect. 5.3.1) for FSR 1716 corresponds to the 7 Gyr, solar-metallicity Padova isochrone, while for Cz 23, we adopted the 5 Gyr, solar-metallicity isochrone (Sect. 5.3.2). The shaded polygon overplotted in *the left panels* shows the colour−magnitude filter.

5. Age, reddening, and distance

Having established that FSR 1716 and Cz 23 present old-age features, we proceed to derive their fundamental parameters. We work with Padova isochrones (Girardi et al. 2002) of solar and sub-solar metallicity, computed with the 2MASS J, H, and K_s filters[6]. These isochrones are very similar to the Johnson-Kron-Cousins ones (e.g. Bessel & Brett 1988), with differences of at most 0.01 in $(J-H)$ (Bonatto et al. 2004). We adopt $R_\odot = 7.2 \pm 0.3$ kpc (Bica et al. 2006a) as the Sun's distance to the Galactic centre to compute the OC's Galactocentric distances. The value $R_\odot = 7.2 \pm 0.3$ kpc was derived by means of the GC spatial distribution. Other recent studies gave similar results, e.g. $R_\odot = 7.2 \pm 0.9$ kpc (Eisenhauer et al. 2003), $R_\odot = 7.62 \pm 0.32$ kpc (Eisenhauer et al. 2005) and $R_\odot = 7.52 \pm 0.10$ kpc (Nishiyama et al. 2006), with different approaches. We make fits *by eye*, taking into account that, because of the presence of binaries, the isochrone should be shifted to the left of the MS fiducial line (e.g. Bonatto et al. 2005, and references therein).

In principle, the decontaminated CMD morphologies (bottom panels of Figs. 3 and 4) – as well as the additional tests discussed in Sect. 4.1 – should provide enough constraints to derive reliable cluster fundamental parameters. However, in view of the importance of identifying new old star clusters, we explore a range of possibilities in terms of age and metallicity. As discussed by, e.g. Friel (1995), OC metallicities in general range from solar ([Fe/H] = 0, or $Z = 0.019$) to sub-solar ([Fe/H] = −0.5, $Z = 0.006$) values.

[6] http://stev.oapd.inaf.it/cgi-bin/cmd

5.1. CMD morphology of FSR 1716

First, we compare in Fig. 7 (top panels) the decontaminated CMD of FSR 1716 to that of the ~7 Gyr OC NGC 188 (Bonatto et al. 2005, and references therein). CMD morphologies in both colours show a good agreement along the MS, MSTO, giant branch, and the MS width, which suggests that both clusters are of similar age. In particular, both CMDs present a similar smoothly-curved MSTO and a scarcely populated red clump.

Different ages and metallicities are tested in Fig. 8 solar-metallicity solutions with isochrones of ages 5, 7, and 9 Gyr are shown in the top-left panel. The same ages but with the low OC metallicity range ([Fe/H] ~ −0.5, which corresponds to $Z \approx 0.006$), are considered in the top-right panels. As a fit constraint, the isochrones have in common a similar description of the MS. In both panels, the youngest isochrone produces a relatively poorer fit, especially to the giant branch. On the other hand, the older isochrones – of both metallicity ranges – produce qualitatively similar fits. This not only confirms the old age of FSR 1716, but, together with a few blue stars at $J \approx 14.3$ and $(J-H) \approx 0.3$ (Fig. 7), which might suggest a blue horizontal branch (HB), raise the possibility of a poorly-populated, metal-poor GC.

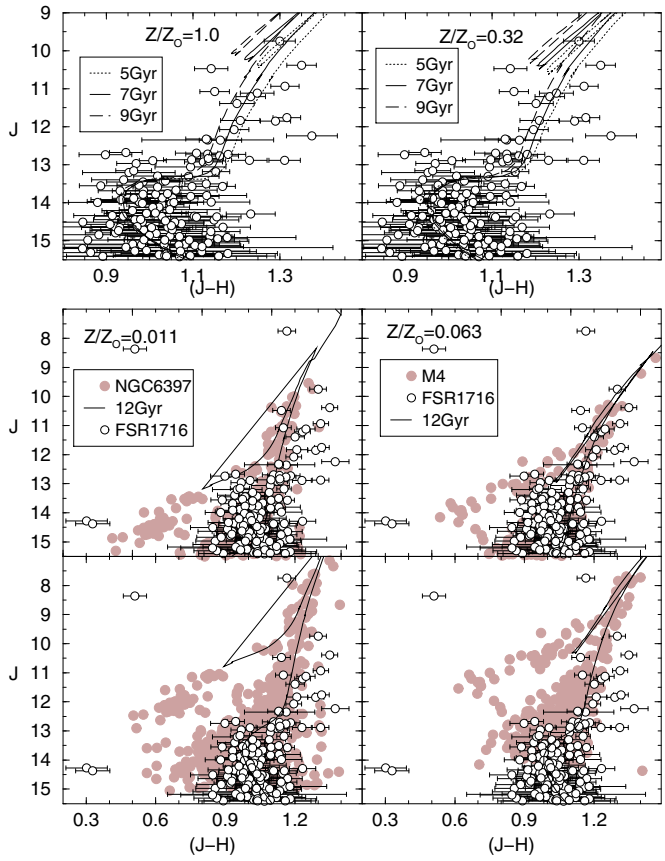

Fig. 8. Age and metallicity interpretation of FSR 1716. *Top-left panel*: isochrones of different ages and fixed solar metallicity. *Top-right*: same ages but with the sub-solar metallicity [Fe/H] = −0.5 (Z = 0.006). Fits have in common a similar description of the MS. *Middle panels*: template fit assuming a GC-like RGB and sub-giant branch morphology for FSR 1716, with the GC NGC 6397 ([Fe/H] = −1.95, Z = 0.0002 – *left panel*), and M 4 ([Fe/H] = −1.21, Z = 0.0012 – *right*). Padova isochrones of 12 Gyr and same metallicity as the GCs are shown. *Bottom panels*: same as above but assuming a brighter MSTO for FSR 1716. The colour range in each panel is optimised to shown differences among the fits (*top*) and enhance the relevant features (*bottom*).

To test the GC hypothesis we compare the decontaminated CMD of FSR 1716 to those of the blue HB GCs NGC 6397 and M 4 (NGC 6121). Both GCs are among the nearest ones ($d_\odot \approx$ 2.3 kpc), which provides MS depth for 2MASS photometry, and are metal-poor, with [Fe/H] ∼ −1.95 (NGC 6397) and [Fe/H] ∼ −1.2 (M 4). We also use Padova isochrones of 12 Gyr to characterise the GC ages (e.g. Ortolani et al. 1995). The CMDs of NGC 6397 (extracted within $R_{\rm ext} < 3'$) and M 4 ($R_{\rm ext} < 2'$) were produced in the same way as those of FSR 1716 (Sect. 3). For a quantitative derivation of fundamental parameters by means of a comparison with GCs, the isochrones were first set to the GCs according to the fundamental data taken from Harris (1996, and the 2003 update[7]). Subsequently, we searched for the best overall match between the GC + isochrone and FSR 1716 sequences. The results are shown in the middle panels of Fig. 8. As a further test, we also searched for solutions with the same isochrones and template GCs as above, but assuming a brighter MSTO for FSR 1716, located at $J \approx$ 13.5. These tentative fits are shown in the bottom panels of Fig. 8[8]. Compared to NGC 6397 (bottom-left panel), the general fit is acceptable, although the RGB of FSR 1716 is somewhat redder, which might suggest a higher metallicity. However, the fit with the more metal-rich GC M 4 (bottom-right) is obviously poorer. Besides the red giants which are too red compared to M 4, the sub-giant branch morphologies clearly are not the same. In the case of the M 4-like solution, FSR 1716 would be as close ($d_\odot \approx$ 0.6 kpc) as an old OC. In the case of the NGC 6397 solution, FSR 1716 would be the nearest ($d_\odot \approx$ 0.5 kpc) GC so far discovered.

The above comparisons show that a very low metallicity, like that of NGC 6397, is not compatible with the giant branch of FSR 1716, since it is steeper and bluer in NGC 6397. M 4, on the other hand, provides a better match for the giant branch. What makes this possibility less likely is that the few extreme blue stars in the CMD of FSR 1716 do not have a counterpart in either NGC 6397 or M 4, whose blue HBs are redder and well distributed in colour. The CMD shape for $13 \lesssim J \lesssim 15$ in FSR 1716 is more compatible with the MSTO and MS of an old OC than the matched subgiant branches of the two GCs. However, the evidence of a Palomar-like (i.e. low-mass and loose structure) GC (Bonatto & Bica 2008a), although marginal, cannot be ruled out with the existing data.

We call attention to the fact that it is not an easy task to establish the nature of a low-mass GC or a low-mass old OC based on a few candidate HB or giant clump stars. For instance, NGC 188 (and other old OCs) presents only a few UV-bright stars, as shown by, e.g. Landsman et al. (1998). In fact, both low-mass GCs and low-mass old OCs hardly have any HBs or clump giants, including NGC 188 with only 5 clump giants (Dinescu et al. 1995; and Landsman et al. 1998). As examples of low-mass GCs with a small number of UV-bright stars we mention Palomar 13 (Côté et al. 2002) with only a few, and AM-4 (Inman & Carney 1987) with none.

Given the above circumstances, deeper observations would be necessary for a more conclusive definition of the nature of FSR 1716 as a GC (as originally suggested by Froebrich et al. 2007a) or a very old OC, with a metallicity that can be sub solar.

5.2. CMD morphology of Cz 23

The CMD features of Cz 23 (bottom panels of Fig. 7) indicate a younger age than FSR 1716. Indeed, its field-decontaminated CMD morphology is similar to that of the old OC M 67. The age of M 67, as derived from near-infrared photometry, is ∼3.2 Gyr (Bonatto & Bica 2003, and references therein). More recent determinations based on spectroscopy of individual stars put the age at ∼4 Gyr (e.g. Giampapa et al. 2006). In addition, the MSTO of Cz 23 seems to be at a slightly fainter magnitude range, which indicates an age older than that of M 67.

Thus, to probe the age and metallicity of Cz 23, we show in Fig. 9 fits with the 3, 5, and 6 Gyr isochrones with a fixed solar metallicity (top panels), and the sub-solar metallicity [Fe/H] ∼ −0.5 (bottom). The fits are required to provide a similar description of the MS. It is clear that, under this condition, the 3 Gyr isochrone fails to reproduce the giant clump, in both metallicity ranges. The 5 and 6 Gyr isochrones, on the other hand, provide acceptable MS and clump fits, which confirms the old age

[7] http://physun.physics.mcmaster.ca/Globular.html

[8] Although at approximately the same distance from the Sun and absorbed by a similar reddening value, the 2MASS cutoffs of M 4 and NGC 6397 are somewhat different. This occurs because M 4 is projected against the bulge ($\ell \approx 351°$), while NGC 6397 lies at the outskirts ($\ell \approx 338°$).

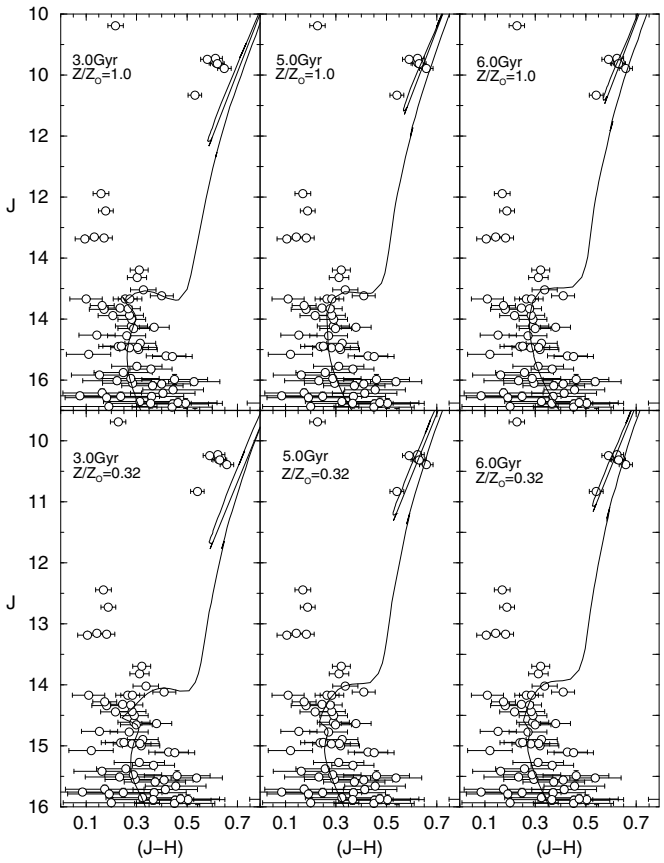

Fig. 9. Age and metallicity interpretation of Cz 23. *Top panels*: isochrones of different ages and fixed solar metallicity. *Bottom*: same ages but with the sub-solar metallicity [Fe/H] = −0.5 (Z = 0.006). Fits are required to provide a similar description of the MS.

of Cz 23. The 6 Gyr solutions are obtained with an essentially zero reddening applied to the isochrones, which implies that older isochrones would require negative correction. This argument constrains the age of Cz 23 to the range ≈4 to ≈6 Gyr.

5.3. The adopted age/metallicity solutions

5.3.1. FSR 1716

Most of the arguments drawn above favour the old OC interpretation for the nature of FSR 1716. Since metal-poor OCs are preferentially distributed in the outer Galaxy (e.g. Friel 1995), and FSR 1716 is located inside the solar circle, its probable metallicity should be around the solar value.

Based on the above, we take the 7 Gyr, solar metallicity isochrone as representative of the stellar sequences of FSR 1716, with an uncertainty of about ±1 Gyr. The corresponding *best-fit* was obtained with the reddening $E(J-H) = 0.63 \pm 0.02$, and observed distance modulus $(m-M)_J = 11.1 \pm 0.2$. This solution is shown in the top panels of Fig. 7. Taking into account fit uncertainties we derive the age 7 ± 1 Gyr, reddening $E(B-V) = 2.0 \pm 0.1$ or, equivalently (Sect. 3) $A_V = 6.3 \pm 0.2$, the absolute distance modulus $(m-M)_O = 9.36 \pm 0.21$, and the distance from the Sun $d_\odot = 0.8 \pm 0.1$ kpc. Thus, for $R_\odot = 7.2$ kpc, the Galactocentric distance of FSR 1716 is $R_{GC} = 6.6 \pm 0.2$ kpc, which puts it ≈0.6 kpc inside the solar circle.

Alternatively, we consider as well the less-likely possibility of a GC. In this case, the *best-fit* of the 12 Gyr isochrone (based on the similarity with the M 4 CMD morphology – Fig. 8) is obtained with $(m-M)_J = 13.5 \pm 0.3$, $E(J-H) = 0.63 \pm 0.04$, $E(B-V) = 2.0 \pm 0.1$ and $A_V = 6.3 \pm 0.2$, $(m-M)_O = 11.76 \pm 0.32$, $d_\odot = 2.3 \pm 0.3$ kpc, and $R_{GC} = 5.4 \pm 0.2$ kpc, thus ≈1.8 kpc inside the solar circle.

5.3.2. Cz 23

With similar arguments as those used to estimate the age of FSR 1716, we take the 5 Gyr (±1 Gyr) isochrone to represent the age of Cz 23. Since both metallicity ranges ([Fe/H] ∼ −0.5 and 0.0) produce similar CMD fits (Fig. 9), for simplicity, we also work with the solar metallicity isochrone.

Thus, fundamental parameters of Cz 23 are $E(J-H) = 0.00 \pm 0.01$, $E(B-V) = 0.00 \pm 0.03$ and $A_V = 0.0 \pm 0.1$, $(m-M)_J = (m-M)_O = 12.0 \pm 0.1$, $d_\odot = 2.5 \pm 0.2$ kpc, and $R_{GC} = 9.7 \pm 0.2$ kpc; Cz 23 lies ≈2.5 kpc outside the solar circle. This solution is shown in the bottom panels of Fig. 7.

6. Cluster structure

Structural parameters are derived by means of the RDPs, defined as the projected radial distribution of the number density of stars around the cluster centre.

Star clusters usually have RDPs that follow a well-defined analytical profile. The most often used are the single mass, modified isothermal sphere (King 1966), the modified isothermal sphere (Wilson 1975), and the power law with a core (Elson et al. 1987). Each function is characterised by different parameters that are related to cluster structure. However, because the error bars in the present RDPs are significant (Fig. 10), we use the analytical profile $\sigma(R) = \sigma_{bg} + \sigma_0/(1 + (R/R_c)^2)$, where σ_{bg} is the residual background density, σ_0 is the central density of stars, and R_c is the core radius. This function is similar to that used by King (1962) to describe the surface brightness profiles in the central parts of globular clusters.

The RDPs are built with colour-magnitude filtered photometry to minimise noise. The most probable cluster sequences are isolated by means of colour–magnitude filters, which are used to exclude stars with colours different from those of the assumed cluster sequence. They are wide enough to include cluster MS and evolved star colour distributions, as well as the 1σ photometric uncertainties. Colour–magnitude filter widths should also account for formation or dynamical evolution-related effects, such as enhanced fractions of binaries (and other multiple systems) towards the central parts of clusters, since such systems tend to widen the MS (e.g. Hurley & Tout 1998; Kerber et al. 2002; Bonatto & Bica 2007b; Bonatto et al. 2005). The colour–magnitude filters for the present OCs are shown in the left panels of Fig. 7. Residual field stars with colours similar to those of the cluster are expected to remain inside the colour–magnitude filter region. They affect the intrinsic stellar RDP in a way that depends on the relative densities of field and cluster stars. The contribution of the residual contamination to the observed RDP is statistically subtracted by means of the field. In practical terms, the use of colour–magnitude filters in cluster sequences enhances the contrast of the RDP with respect to the background, especially for clusters in dense fields (e.g. Bonatto & Bica 2007b).

Oversampling near the centre and undersampling at large radii are avoided by using rings of increasing width with distance from the centre. A typical set of ring widths is ΔR = 0.5, 1, 2, and 5′, respectively for $0' \le R < 1'$, $1' \le R < 4'$, $4' \le R < 10'$, and $10' \le R < 30'$. The number and width

Table 3. Cluster structural parameters.

Cluster	1′ (pc)	σ_{bg} (stars arcmin^{-2})	σ_0 (stars arcmin^{-2})	δ_c	R_c (′)	R_{RDP} (′)	R_c (pc)	R_{RDP} (pc)
(1)	(2)	(3)	(4)	(5)	(6)	(7)	(8)	(9)
FSR 1716†	0.216	10.5 ± 1.0	16.2 ± 4.8	2.6 ± 0.5	0.88 ± 0.23	6.0 ± 0.6	0.19 ± 0.05	1.3 ± 0.2
FSR 1716‡	0.653	10.5 ± 1.0	16.2 ± 4.8	2.6 ± 0.5	0.88 ± 0.23	6.0 ± 0.6	0.57 ± 0.15	3.9 ± 0.4
Cz 23	0.728	2.8 ± 0.1	16.5 ± 4.7	7.0 ± 1.7	0.49 ± 0.04	4.9 ± 0.7	0.36 ± 0.08	3.6 ± 0.4

Notes. Column 2: arcmin to parsec scale. King profile is expressed as $\sigma(R) = \sigma_{bg} + \sigma_0/(1+(R/R_c)^2)$. To minimise degrees of freedom in RDP fits, σ_{bg} was kept fixed (measured in the respective comparison fields) while σ_0 and R_c were allowed to vary. Column 5: cluster/background density contrast ($\delta_c = 1 + \sigma_0/\sigma_{bg}$), measured in CM-filtered RDPs. Columns 6–9, core and cluster radii in angular and absolute units. Parameters of FSR 1716 are derived for the OC (†) or GC (‡) interpretation (Sect. 5).

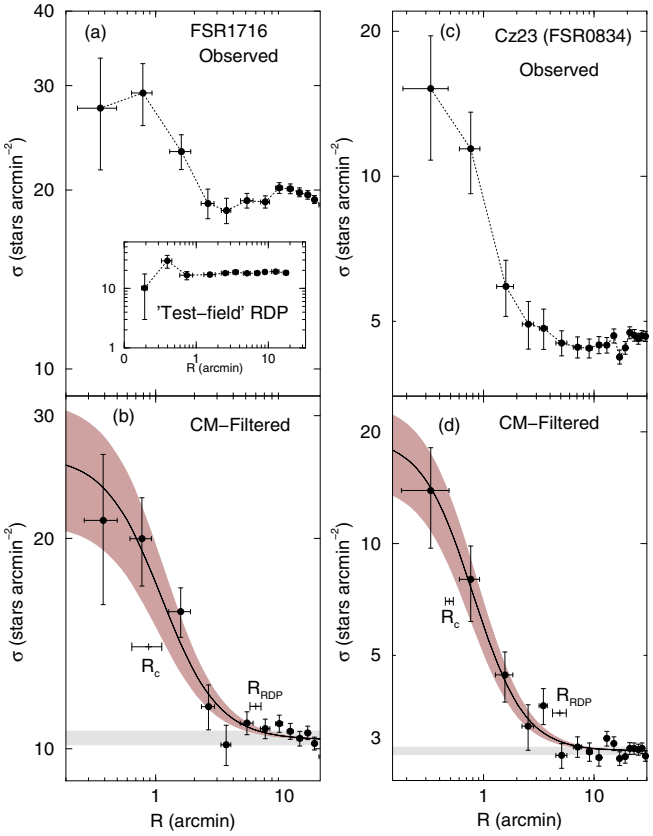

Fig. 10. Stellar RDPs (filled circles) of FSR 1716 (*left panels*) and Cz 23 (*right*). RDPs built with the observed (raw) photometry are shown in *the top panels*, while those built with colour–magnitude filtered photometry are in *the bottom panels*. Solid line: best-fit King-like profile. Horizontal shaded polygon: offset field stellar background level. Shaded regions: 1σ King fit uncertainty. The core and cluster radii are indicated. Inset of panel **a**): RDP of the test-field of FSR 1716. Angular scale is used.

of the rings can be set to produce RDPs with adequate spatial resolution and as low as possible 1σ Poisson errors. The residual background level of each RDP corresponds to the average number of colour–magnitude filtered stars measured in the field. The R coordinate (and uncertainty) of each ring corresponds to the average position and standard deviation of the stars inside the ring.

The RDPs of FSR 1716 and Cz 23 are given in Fig. 10. Because of the uncertainties associated with the age (and metallicity) derivations (Sect. 5), which propagate to the absolute value of the structural parameters, RDPs in Fig. 10 are shown on an angular scale. Besides the RDPs built with the colour–magnitude filters, we show, for illustrative purposes, those produced with the observed (raw) photometry. Especially for FSR 1716, minimisation of the number of non-cluster stars by the colour–magnitude filter resulted in a RDP with a higher contrast with respect to the background. Fits of the King-like profile were performed with a non-linear least-squares fit routine that uses errors as weights. To minimise degrees of freedom, σ_0 and R_c were derived from the RDP fit, while σ_{bg} is measured in the field. These values are given in Table 3, and the best-fit solutions are superimposed on the colour–magnitude filtered RDPs (Fig. 10). Table 3 also provides structural parameters in absolute units, computed with the cluster distances derived in Sect. 5.3. Because of the 2MASS photometric limit, which in most cases corresponds to a cutoff for stars brighter than $J \approx 16$, σ_0 should be taken as a lower limit to the actual central number density. The adopted King-like function well describes the RDPs along the full radius range, within uncertainties.

To complete the structural description of the clusters we also estimate the cluster radius (R_{RDP}) and uncertainty by visually comparing the RDP level (and fluctuations) with the background. The cluster radius corresponds to the distance from the cluster centre where the RDP and background are statistically indistinguishable (e.g. Bonatto & Bica 2005, and references therein). For practical purposes, most of the cluster stars are contained within R_{RDP}. Note that R_{RDP} should not be mistaken for the tidal radius. Tidal radii are derived from King fits to RDPs, which depend on wide fields and adequate Poisson errors. For instance, in populous and relatively high Galactic latitude OCs such as M 67, NGC 188, and NGC 2477, cluster radii are a factor ~0.5–0.7 of the respective tidal radii (Bonatto & Bica 2005). The cluster radii of the present objects are given in Cols. 6, 7 (angular scale) and 8, 9 (absolute scale) of Table 3. If cluster and tidal radii of FSR 1716 and Cz 23 are similarly related as in the bright OCs, the lower-limit of the radial range taken as a comparison field (Sect. 4) is located beyond the probable tidal radius. This, in turn, minimises the probability of cluster members at large radii, e.g. in the cluster halo, being considered as field stars by the decontamination algorithm.

Compared to the distribution of core radius derived for a sample of relatively nearby OCs by Piskunov et al. (2007), FSR 1716 (especially the OC interpretation) and Cz 23 occupy the small-R_c tail. Assuming that the tidal radius is ~2 × R_{RDP}, Cz 23 and FSR 1716 (GC interpretation) would be around the median value of the distribution, while the OC interpretation of FSR 1716 again would be at the small tidal radius tail.

Table 3 (Col. 5) provides the density contrast parameter $\delta_c = 1 + \sigma_0/\sigma_{bg}$. Since δ_c is measured in colour–magnitude-filtered RDPs, it may not correspond to the visual contrast produced by observed stellar distributions in images. FSR 1716 presents a low contrast in the 2MASS K_s image (Fig. 1) but, because most of the non-cluster stars have been excluded by the colour–magnitude

filter, the corresponding RDP has a relatively high density contrast, $\delta_c \approx 2.6$. Obviously, the high-contrast OC Cz 23 (Figs. 1 and 10) is reflected in the high value of the density-contrast parameter $\delta_c \approx 7.0$. Interestingly, FSR 1716 and Cz 23 are projected against almost opposite regions (Table 1). Accordingly, the background (including foreground) stellar contribution turns out to be ≈11 stars arcmin^{-2} in the direction of FSR 1716, and ≈2.8 stars arcmin^{-2} towards Cz 23.

Finally, the RDP of the "test-field" of FSR 1716 is shown in the inset of panel (a) of Fig. 10. As expected from the CMD analysis (Sect. 4.1), the RDP is uniform from the centre to the borders of the field, characterised essentially by Poisson fluctuations. The featureless "test-field" RDP is low and flat, as compared the cluster RDP of FSR 1716 (panels a and c).

7. Mass function and cluster mass estimate

The cluster mass functions $\left(\phi(m) = \frac{dN}{dm}\right)$ are built following the methods presented in Bonatto & Bica (2005) (and references therein). We build them with colour−magnitude filtered photometry, the 3 2MASS bands separately, and the mass-luminosity relations obtained from the Padova isochrones and distances from the Sun adopted for FSR 1716 (Sect. 5.3.1) and Cz 23 (Sect. 5.3.2). Further details on MF construction are given in Bica et al. (2006b). The effective magnitude range over which MFs are computed is that where clusters present an excess of stars over the field. In both cases it begins below the MSTO and ends at a faint magnitude limit brighter than that stipulated by the 2MASS completeness limit (Sect. 3). The effective MS stellar mass ranges are $0.83 \leq m(M_\odot) \leq 1.1$ (FSR 1716), and $0.94 \leq m(M_\odot) \leq 1.2$ (Cz 23).

The MFs computed for the whole cluster region ($R < R_{RDP}$) are shown in Fig. 11. Both cases suggest important depletion of the low-mass content, suggesting advanced dynamical evolution, especially in the case of FSR 1716. The drop in the MF of FSR 1716 begins at $m \lesssim 0.98\ M_\odot$, which corresponds to $J \approx 14.5$, more than 1 mag brighter than the 2MASS 99.9% completeness limit (Sect. 3) at the cluster position. This suggests that the drop may be real, although we cannot rule out crowding to account for part of the important MF drop, since the 2MASS completeness limits refer to the field. Bearing in mind this caveat, we fit the MF of FSR 1716 with a two-segment function, $\phi(m) \propto m^{-(1+\chi)}$, with $\chi = -9.4 \pm 0.6$ in the mass range $m \leq 0.98\ M_\odot$, and $\chi = 2.3 \pm 0.4$ for $0.98 < m(M_\odot) < 1.1$. The high-mass range slope is, within the uncertainty, somewhat steeper than the $\chi = 1.35$ of the Salpeter (1955) Initial Mass Function (IMF). However, the low-mass range slope is much flatter than Salpeter's IMF. The drop in the MF of FSR 1716 (at $m \approx 1\ M_\odot$) agrees with one of the breaks present in the universal IMF of Kroupa (2001), which assumes increasing flattening towards low-mass stars. This IMF is described by the slopes $\chi = 0.3 \pm 0.5$ for the range $0.08 \leq m(M_\odot) \leq 0.5$ and $\chi = 1.3 \pm 0.3$ for $0.5 \leq m(M_\odot) \leq 1.0$. The low-mass range of the MF of FSR 1716 is flatter than Kroupa's IMF, which again points to advanced dynamical evolution, crowding or, more probably, a combination of both.

Although flat, the MF of Cz 23 is more monotonic than that of FSR 1716, and can be described by a single power-law, with the slope $\chi = -3.1 \pm 0.5$, also flatter than Salpeter's or Kroupa's IMF.

The number of observed MS and evolved stars in FSR 1716 is derived by counting the number of stars (in the background-subtracted colour−magnitude filtered photometry) that lie in the corresponding magnitude ranges, $13.4 < J < 15.4$ for the MS

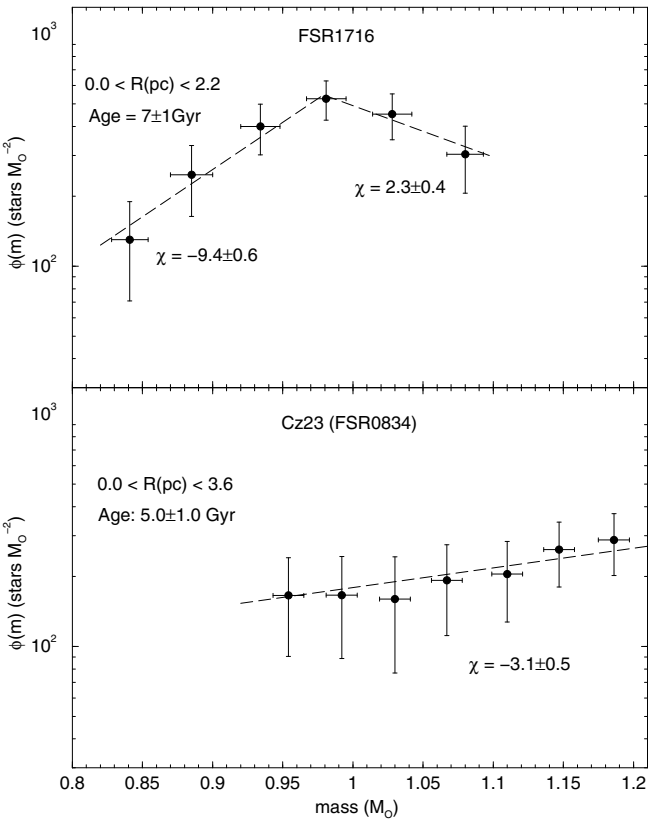

Fig. 11. Mass function computed for the whole region of FSR 1716 (*top panel*) and Cz 23 (*bottom*). The MF of FSR 1716 can be represented by the broken power-law $\phi(m) \propto m^{-(1+\chi)}$, with $\chi = -9.4 \pm 0.6$ for $m \leq 0.98\ M_\odot$, and $\chi = 2.3 \pm 0.4$ for $0.98 < m(M_\odot) < 1.1$. The MF drop begins at $m \approx 0.98\ M_\odot$, which corresponds to $J \approx 14.5$. The MF of Cz 23 can be described by a power-law with slope $\chi = -3.1 \pm 0.5$.

and $J < 13.4$ for the evolved stars. There are $n_{MS} = 99 \pm 5$ and $n_{evol} = 53 \pm 7$, MS and evolved stars, respectively; the corresponding mass values are $m_{MS} = 97 \pm 5\ M_\odot$ and $m_{evol} = 58 \pm 8\ M_\odot$. The evolved star mass corresponds to n_{evol} multiplied by the stellar mass at the MSTO, $m_{TO} = 1.1\ M_\odot$. To estimate the total stellar mass we extrapolate the observed MF down to the H-burning mass limit (0.08 $M_\odot$). Because of the very flat slope at the low-mass range, the extrapolated values are similar to the observed ones, $n_{extr} = 160 \pm 8$ and $m_{extr} = 160 \pm 9\ M_\odot$.

The number of MS and evolved stars in Cz 23 is $n_{MS} = 54 \pm 4$ and $n_{evol} = 5 \pm 3$, and the respective masses are $m_{MS} = 60 \pm 4\ M_\odot$ and $m_{evol} = 7 \pm 4\ M_\odot$; the extrapolated values are $n_{extr} = 120 \pm 8$ and $m_{extr} = 115 \pm 7\ M_\odot$.

Presently, both FSR 1716 and Cz 23 appear to be low-mass OCs, even when stars less massive than the observed range are taken into account. Most of the original mass must have been lost to the field because of dynamical effects during the several Gyr since their formation (Sect. 8).

8. Discussion

The range of acceptable isochrone solutions (Sect. 5), together with the statistical tests (Sect. 4) applied to FSR 1716 and Cz 23, i.e. *(i)* the decontamination algorithm; *(ii)* the integrated and per magnitude $N_{1\sigma}$ parameter; and *(iii)* the ratio of N_{cl} to σ_{FS}, produce results consistent with both objects being old OCs. Examination of photometric and structural properties of the

offset "test-fields" for FSR 1716 and Cz 23 also leads to the same conclusion.

With the analyses of the preceding sections, we provide fundamental and structural parameters, most of which are given for the first time for FSR 1716 and Cz 23. We now use these parameters to compare some of their properties with those of a set of well-studied OCs.

We compare the structural parameters, computed with the adopted isochrone solutions for FSR 1716 (Sect. 5.3.1) and Cz 23 (Sect. 5.3.2), with those of a reference sample of nearby OCs with ages in the range 70−7000 Myr and masses within 400−5300 $M_{\odot}$ (Bonatto & Bica 2005). To the original reference sample were added the young OCs NGC 6611 (Bonatto et al. 2006c) and NGC 4755 (Bonatto et al. 2006b). Clusters are distinguished according to total mass (lower or higher than 1000 $M_{\odot}$). Bonatto & Bica (2005) discuss parameter correlations in the reference sample. For completeness, both sets of parameters for FSR 1716 (Table 3), corresponding to the old OC and GC possibilities, are considered separately.

Core and cluster radii of the reference sample relate as $R_{\rm RDP} = (8.9 \pm 0.3) \times R_{\rm c}^{(1.0\pm0.1)}$ (panel a), which suggests a similar scaling for both kinds of radii, at least for the sampled ranges of $0.25 \lesssim R_{\rm c}({\rm pc}) \lesssim 1.5$ and $2 \lesssim R_{\rm RDP}({\rm pc}) \lesssim 15$. Within the uncertainties, FSR 1716 (both interpretations) and Cz 23 fit tightly into that relation.

The reference OCs appear to follow the trend of increasing cluster radii with Galactocentric distance (panel b), a dependence previously suggested by e.g. Lyngå (1982). To explain the increase of GC radii with Galactocentric distance, van den Bergh et al. (1991) suggested that part of the relation may be primordial, in the sense that the higher molecular gas density in central Galactic regions may have produced clusters with small radii. After formation, mass loss associated with stellar and dynamical evolution (such as mass segregation and evaporation), together with tidal interactions with the Galactic potential and giant molecular clouds, also contribute to the depletion of star clusters, especially the low-mass and centrally located ones (Sect. 1). The cluster radius of FSR 1716 (GC interpretation) is consistent with the assumed relation. On the other hand, Cz 23, and the OC interpretation of FSR 1716, appear exceedingly small for their Galactocentric distance, which is consistent with the several Gyr of depletion. A similar dependence on Galactocentric distance holds as well for $R_{\rm c}$, because of the relation to $R_{\rm RDP}$implied by panel (a).

In panels (c) and (d) of Fig. 12 we compare the cluster and core radii of FSR 1716 and Cz 23 with those of the reference sample in terms of age. The locus occupied by Cz 23 in both panels is consistent with the corresponding radii measured in low-mass, old OCs. A similar conclusion applies to the GC interpretation of FSR 1716 (which again would be consistent with the structural parameters of Palomar-like GCs – Bonatto & Bica 2008a). The significantly small radii of the OC interpretation of FSR 1716, especially $R_{\rm RDP}$, are consistent with those of OCs that have suffered severe depletion effects for long periods (e.g. Bonatto & Bica 2005; Bonatto & Bica 2007a, and references therein).

Further evidence in favour of dynamical effects affecting cluster size comes from the positions of FSR 1716 and Cz 23 in the Galactic plane (Fig. 13). The Milky Way's spiral arm structure is based on Momany et al. (2006) and Drimmel & Spergel (2001), derived from HII regions and molecular clouds (e.g. Russeil 2003). The Galactic bar is shown with a 14° orientation and 3 kpc in length (Freudenreich 1998; Vallée 2005). For comparison, we also include WEBDA clusters younger and older than 1 Gyr. As discussed in Sect. 1, old OCs are distributed preferentially outside the solar circle.

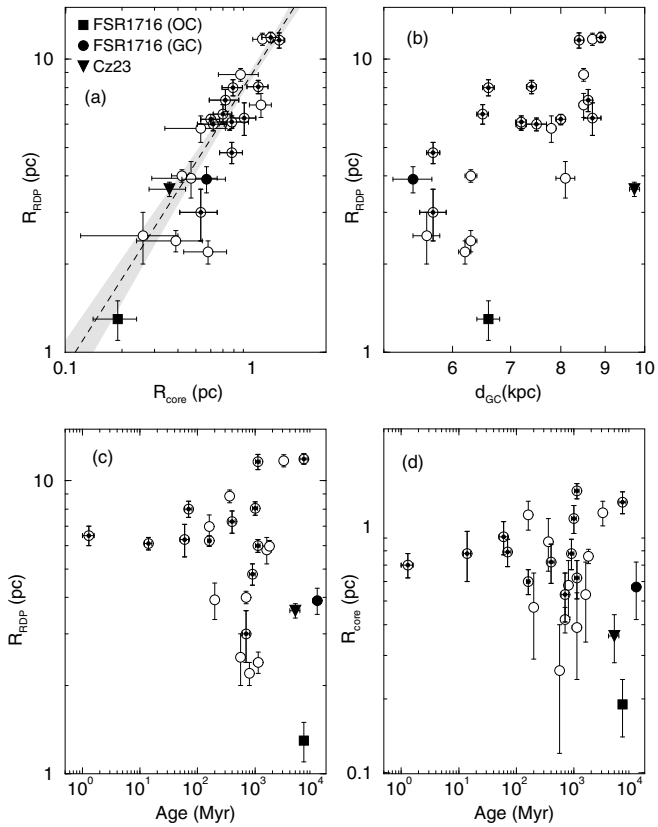

Fig. 12. Relations involving OC structural and fundamental parameters. Circles: nearby OCs. Dotted circles: massive OCs (>1000 $M_{\odot}$). Two sets of parameters are shown for FSR 1716, according to the old OC and GC solutions.

Interestingly, both clusters occur close to spiral arms, Cz 23 on Perseus, and FSR 1716 on Carina-Sagittarius (OC interpretation) or Crux-Scutum (GC). Since they are located close to the plane (Table 1), they may have interacted with the arms, especially by means of encounters with giant molecular clouds[9]. As discussed above, part of the small sizes of FSR 1716 and Cz 23 can be accounted for by collisions with such structures (e.g. Wielen 1971; Wielen 1991; Gieles et al. 2006; Gieles et al. 2007). A similar effect was recently observed to occur with some small OCs located close to the Local and Orion-Cygnus Arms (Bonatto & Bica 2008b).

Finally, both objects have MFs that appear to be very eroded and flat which, given the discussion on structural parameters above, reflects the consequences of several Gyr of the relentless dynamical effects and mass loss due to stellar evolution. Also, both objects are low-mass clusters, with less than ~200 $M_{\odot}$ presently stored in stars. They must have been formed as more massive open clusters to have survived for so long in the Galaxy.

9. Concluding remarks

In this paper we studied the nature of two stellar overdensities included in the catalogue of candidate star clusters of Froebrich et al. (2007a), FSR 1716 and FSR 834. The former was suggested to be a globular cluster candidate by

[9] Molecular clouds more massive than ~10^6 $M_{\odot}$ are found in the solar neighbourhood (e.g. Solomon et al. 1987).

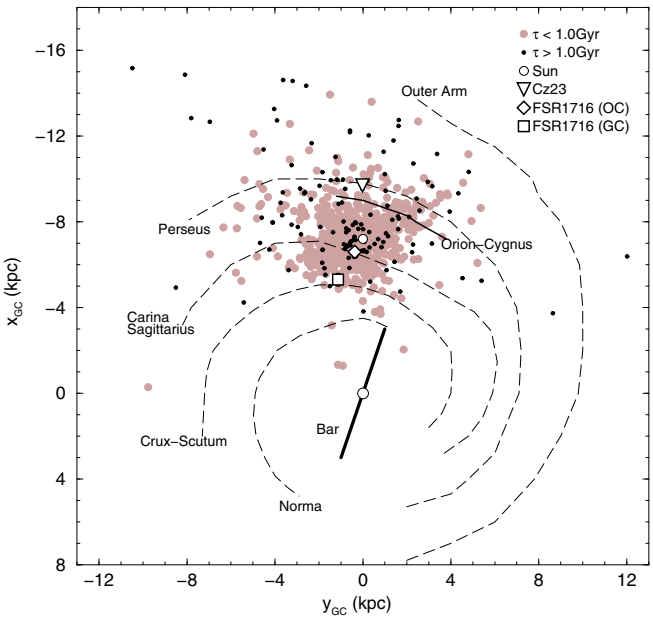

Fig. 13. Galactic position of FSR 1716 and Cz 23 compared to the WEBDA OCs with ages younger (shaded circles) and older (filled circles) than 1 Gyr. The schematic projection of the Galaxy is seen from the North pole, with 7.2 kpc as the Suns distance to the Galactic centre. Main structures are identified.

Froebrich et al. (2007a), while the latter has the OC Cz 23 as optical counterpart. The analyses are based on field-star decontaminated 2MASS CMDs and stellar radial density profiles, with algorithms previously constructed by our group. Fundamental and structural parameters of the clusters are derived.

We present consistent evidence (e.g. CMD morphology, statistical tests, structural parameters, mass-function slope, and comparison with nearby OCs) that both objects are old star clusters.

FSR 1716 is significantly absorbed ($A_V \approx 6.3$) and projected not far from the bulge. Its field-decontaminated CMD morphology is very similar to that of the ∼7 Gyr well-known OC NGC 188. Indeed, its CMD can be well represented by isochrones with ages older than ∼6 Gyr, both of solar and sub-solar ([Fe/H] ∼ −0.5) metallicity. We adopted the former as the metallicity of FSR 1716, because of its relatively central location. Alternatively, we cannot rule out the possibility that FSR 1716 is a low-mass, loose (Palomar-like) globular cluster. FSR 1716 is located inside the solar circle, ≈0.6 kpc (in the case of an OC) or ≈1.8 kpc (GC).

The CMD morphology of Cz 23 is consistent with that of the ∼4 Gyr old OC M 67. Similarly to FSR 1716, it can be well represented by solar and sub-solar metallicity isochrones, but with ages in the range 4–6 Gyr. With the ≈5 Gyr and solar metallicity solution, we find that Cz 23 is projected nearly towards the anti-centre, located ≈2.5 kpc outside the solar circle.

The core and cluster radii of FSR 1716 and Cz 23 are small when compared to a set of open clusters in the solar neighbourhood. However, such radii are comparable to those of other OCs of similar old age. Also, the mass functions appear to be much flatter than Salpeter's IMF, especially FSR 1716, which seems to present an increasing depletion in the number of low-mass stars. As a consequence, the total mass presently stored in stars in both clusters is lower than ∼200 $M_\odot$. Such a low value probably reflects the several Gyr-long period of mass loss due to stellar evolution, tidal interactions with the bulge (possibly in the case of FSR 1716), disk and giant molecular clouds. Because of its low mass content and flat mass function, Cz 23 may be evolving into an open cluster remnant (e.g. Pavani & Bica 2007).

Comprehensive catalogues of star cluster candidates, such as that of Froebrich et al. (2007a), should be further explored with field-star decontamination algorithms and other tools, so that the nature of the candidates can be probed and the age derived. It is remarkable how the decontamination tool unveiled the intrinsic CMD sequences of FSR 1716, separating it from the crowded field population. Consequently, the characterisation of FSR 1716 and Cz 23 as OCs older than ∼4 Gyr represents an important increase (≈10%) in the known population of such objects in the Galaxy. In particular, FSR 1716 is the most recent addition to the 8 open clusters older than 6 Gyr so far identified (WEBDA). In this sense, Cz 23 (FSR 834), and especially FSR 1716, can be considered as rare examples of extreme dynamical survivors in disk-regions where most open clusters are short-lived.

Acknowledgements. We thank the anonymous referee for helpful suggestions. This publication makes use of data products from the Two Micron All Sky Survey, which is a joint project of the University of Massachusetts and the Infrared Processing and Analysis Centre/California Institute of Technology, funded by the National Aeronautics and Space Administration and the National Science Foundation. This research has made use of the WEBDA database, operated at the Institute for Astronomy of the University of Vienna. We acknowledge support from the Brazilian Institution CNPq.

References

Baumgardt, H., & Makino, J. 2003, MNRAS, 340, 227
van den Bergh, S. 1957, ApJ, 125, 445
van den Bergh, S., Morbey, C., & Pazder, J. 1991, ApJ, 375, 594
Bessel, M. S., & Brett, J. M. 1988, PASP, 100, 1134
Bica, E., & Bonatto, C. 2008, MNRAS, 384, 1733
Bica, E., Bonatto, C., Barbuy, B., & Ortolani, S. 2006a, A&A, 450, 105
Bica, E., Bonatto, C., & Blumberg, R. 2006b, A&A, 460, 83
Bica, E., Bonatto, C., Ortolani, S., & Barbuy, B. 2007, A&A, 472, 483
Bica, E., Bonatto, C., & Camargo, D. 2008, MNRAS, 385, 349
Bonatto, C., & Bica, E. 2003, A&A, 405, 525
Bonatto, C., & Bica, E. 2005, A&A, 437, 483
Bonatto, C., & Bica, E. 2007a, A&A, 473, 445
Bonatto, C., & Bica, E. 2007b, MNRAS, 377, 1301
Bonatto, C., & Bica, E. 2008a, A&A, 479, 741
Bonatto, C., & Bica, E. 2008b, A&A, 485, 81
Bonatto, C., Bica, E., & Girardi, L. 2004, A&A, 415, 571
Bonatto, C., Bica, E., & Santos, Jr., J. F. C. 2005, A&A, 433, 917
Bonatto, C., Kerber, L. O., Bica, E., & Santiago, B. X. 2006a, A&A, 446, 121
Bonatto, C., Bica, E., Ortolani, S., & Barbuy, B. 2006b, A&A, 453, 121
Bonatto, C., Santos, Jr., J. F. C., & Bica, E. 2006c, A&A, 445, 567
Bonatto, C., Bica, E., Ortolani, S., & Barbuy, B. 2007, MNRAS, 381, L45
Cardelli, J. A., Clayton, G. C., & Mathis, J. S. 1989, ApJ, 345, 245
Carraro, G., Janes, K. A., Costa, E., & Méndez, R. A. 2006, MNRAS, 368, 1078
Côté, P., Djorgovski, S. G., Meylan, G., Castro, S., & McCarthy, J. K. 2002, ApJ, 574, 783
Czernik, M. 1966, AcA, 16, 93
Dinescu, D. I., Demarque, P., Guenther, D. B., & Pinsonneault, M. H. 1995, AJ, 109, 2090
Drimmel, R., & Spergel, D. N. 2001, ApJ, 556, 181
Dutra, C. M., Santiago, B. X., & Bica, E. 2002, A&A, 383, 219
Eisenhauer, F., Schödel, R., Genzel, R., et al. 2003, ApJ, 597, L121
Eisenhauer, F., Genzel, R., Alexander, T., et al. 2005, ApJ, 628, 246
Elson, R. A. W., Fall, S. M., & Freeman, K. C. 1987, ApJ, 323, 54
Freudenreich, H. T. 1998, ApJ, 492, 495
Friel, E. D. 1995, ARA&A, 33, 381
Froebrich, D., Scholz, A., & Raftery, C. L. 2007a, MNRAS, 374, 399
Froebrich, D., Meusinger, H., & Scholz, A. 2007b, MNRAS, 377, L54
Froebrich, D., Meusinger, H., & Davis, C. J. 2008, MNRAS, 383, L45
Giampapa, M. S., Hall, J. C., Radick, R. R., & Baliunas, S. L. 2006, ApJ, 651, 444

Gieles, M., Portegies Zwart, S. F., Baumgardt, H., et al. 2006, MNRAS, 371, 793
Gieles, M., Athanassoula, E., & Portegies Zwart, S. F. 2007, MNRAS, 376, 809
Girardi, L., Bertelli, G., Bressan, A., et al. 2002, A&A, 391, 195
Goodwin, S. P., & Bastian, N. 2006, MNRAS, 373, 752
Harris, W. E. 1996, AJ, 112, 1487
von Hoerner, S. 1958, Astrophys., 44, 221
Hurley, J., & Tout, A. A. 1998, MNRAS, 300, 977
Inman, R. T., & Carney, B. W. 1987, AJ, 93, 1166
Kerber, L. O., Santiago, B. X., Castro, R., & Valls-Gabaud, D. 2002, A&A, 390, 121
Khalisi, E., Amaro-Seoane, P., & Spurzem, R. 2007, MNRAS, 374, 703
King, I. 1962, AJ, 67, 471
King, I. 1966, AJ, 71, 64
Kroupa, P. 2001, MNRAS, 322, 231
Landsman, W., Bohlin, R. C., Neff, S. G., et al. 1998, AJ, 116, 789
Lamers, H. J. G. L. M., & Gieles, M. 2006, A&AL, 455, 17
Lyngå, G. 1982, A&A, 109, 213
Mercer, E. P., Clemens, D. P., Meade, M. R., et al. 2005, ApPJ, 6335, 560
Mermilliod, J. C., & Paunzen, E. 2003, A&A, 410, 511
Momany, Y., Zaggia, S., Gilmore, G., et al. 2006, A&A, 451, 515
Nishiyama, S., Nagata, T., Sato, S., et al. 2006, ApJ, 647, 1093
Oort, J. H. 1958, in Specola Vaticana, Proc. of a Conference at Vatican Observatory, Castel Gandolfo, May 20−28, 1957, ed. D. J. K. O'Connell, Ricerche Astron., 5, 415
Ortolani, S., Renzini, A., Gilmozzi, R., et al. 1995, Nature, 377, 701
Ortolani, S., Bica, E., Barbuy, B., & Zocalli, M. 2005a, A&A, 439, 1135
Ortolani, S., Bica, E., & Barbuy, B. 2005b, A&A, 437, 531
Pavani, D. N., & Bica, E. 2007, MNRAS, 468, 139
Piskunov, A. E., Kharchenko, N. V., Röser, S., Schilbach, E., & Scholz, R.-D. 2007, A&A, 445, 545
Portegies Zwart, S. F., Makino, J., McMillan, S. L. W., & Hut, P. 2002, ApJ, 565, 265
Ruprecht, J. 1966, BAICz, 17, 33
Russeil, D. 2003, A&A, 397, 133
Salaris, M., Weiss, A., & Percival, S. M. 2004, A&A, 422, 217
Salpeter, E. 1955, ApJ, 121, 161
Skrutskie, M., Schneider, S. E., Stiening, R., et al. 1997, in The Impact of Large Scale Near-IR Sky Surveys, ed. Garzon et al. (The Netherlands: Kluwer), ASSL, 210, 187
Solomon, P. M., Rivolo, A. R., Barrett, J., & Yahil, A. 1987, ApJ, 319, 730
Spitzer, L. 1958, ApJ 127, 17
Upgren, A. R., Mesrobian, W. S., & Kerridge, S. J. 1972, AJ, 77, 74
Vallée, J. P. 2005, AJ, 130, 569
Wielen, R. 1971, A&A, 13, 309
Wielen, R. 1991, in The Formation and Evolution of Star Clusters, ed. K. Janes, ASP Conf. Ser., 13, 343
Wilson, C. P. 1975, AJ, 80, 175